Journal of Materials Chemistry C

PAPER

View Article Online
View Journal | View Issue

Cite this: J. Mater. Chem. C, 2017, 5, 9359

Ultralow percolation threshold and enhanced electromagnetic interference shielding in poly(L-lactide)/multi-walled carbon nanotube nanocomposites with electrically conductive segregated networks†

Kai Zhang,[a] Gen-Hui Li,[a] La-Mei Feng,[a] Ning Wang,[b] Jiang Guo,[c] Kai Sun,[c] Kai-Xin Yu,[a] Jian-Bing Zeng,[a] Tingxi Li,*[d] Zhanhu Guo *[c] and Ming Wang *[a]

Received 30th June 2017,
Accepted 31st July 2017

DOI: 10.1039/c7tc02948a

rsc.li/materials-c

Electrically conductive segregated networks were built in poly(L-lactide)/multi-walled carbon nanotube (PLLA/MWCNT) nanocomposites without sacrificing their mechanical properties *via* simply choosing two different PLLA polymers with different viscosities and crystallinities. First, the MWCNTs were dispersed in PLLA with low viscosity and crystallinity (L-PLLA) to obtain the L-PLANT phase. Second, the PLLA particles with high viscosity and crystallinity (H-PLLA) were well coated with the L-PLANT phase at 140 °C which was below the melting temperature of H-PLLA. Finally, the coated H-PLLA particles were compressed above the melting temperature of H-PLLA to form the PLLA/MWCNT nanocomposites with segregated structures. The morphological observation showed the successful location of MWCNTs in the continuous L-PLLA phase, resulting in an ultralow percolation threshold of 0.019 vol% MWCNTs. The electrical conductivity and the electromagnetic interference (EMI) shielding effectiveness (SE) of the composites with the segregated structure are 25 S m^{-1} and ~30 dB, showing three orders and 36% higher than that of the samples with a random distribution of MWCNTs with 0.8 vol% of MWCNT loading, respectively. High-performance electromagnetic interference (EMI) shielding was also observed mainly dependent on the highly efficient absorption shielding, which can be achieved by the densely continuous MWCNT networks and the abundant interfaces induced by the segregated structures. Furthermore, the composites with segregated structures not only showed higher Young's modulus and tensile strength than the corresponding conventional composites, but also maintained high elongation at break because of the continuous and dense MWCNT networks induced by the segregated structures and the high interfacial interaction between H-PLLA and L-PLLA.

Introduction

Electronic technology, including computers, mobile phones, the Internet, and electronic organizers, brings much convenience in our daily life. However, electromagnetic (EM) radiation, which can be generated by using electronic technology, is harmful to electronic devices and human beings.[1–6] Recently, conductive materials with electromagnetic interference (EMI) shielding have attracted considerable attention for civil, commercial, military, and aerospace applications.[7–12] Among the EMI materials, conductive polymer composites (CPCs) exhibit many advantages, such as light weight, tunable conductivity, resistance to corrosion, and good processability.[13–16] Normally, the electrical conductivity and EMI shielding efficiency of CPCs depend mainly on the conductive networks formed by adding conductive fillers.[17–20] The formation of conductive networks has been considered to be related to filler loadings. The percolation threshold (ϕ_c) which is the critical content of conductive fillers with insulator/conductor transition is used to indicate the formation of conductive networks.[21–27] However, high ϕ_c is usually found in conventional composites to form conductive networks.

[a] Key Laboratory of Applied Chemistry of Chongqing Municipality, School of Chemistry and Chemical Engineering, Southwest University, Chongqing, 400715, China. E-mail: mwang@swu.edu.cn
[b] Engineered Multifunctional Composites (EMC) Nanotechnology LLC, Knoxville, TN, 37934, USA
[c] Integrated Composites Laboratory (ICL), Department of Chemical and Biomolecular Engineering, University of Tennessee, Knoxville, TN, 37996, USA. E-mail: nanomaterials2000@gmail.com, zguo10@utk.edu
[d] College of Materials Science and Engineering, Shandong University of Science and Technology, Qingdao 266590, China. E-mail: litx@sdust.edu.cn

† Electronic supplementary information (ESI) available. See DOI: 10.1039/c7tc02948a

This high content of conductive fillers always leads to poor processability, low economic affordability and inferior mechanical properties.[28–30]

Recently, the percolation threshold has been greatly reduced by controlling the distribution of conductive fillers in polymer matrices.[31–46] For example, double percolation structures can be formed in a co-continuous immiscible polymer blend with conductive fillers selectively located in one continuous phase or interfaces.[31–34] As a result, the electrical conductivity and EMI shielding performance can be significantly enhanced with a low percolation threshold.[35] However, it is still a great challenge to fabricate high-efficient double percolation structures through the conventional blending method.[36] In the past decade, a facile controllable strategy based on segregated structures has been demonstrated to be an efficient approach to improve the electrical conductivity and EMI shielding performance with ultra-low percolation threshold.[37–42] The conductive fillers can be easily located at the interfaces of polymer particles to construct dense conductive networks.[43] However, the dense conductive fillers at interfacial layers will lead to hard fusion of the polymer particles and be harmful to the formation of high-performance CPCs. In addition, the agglomerates of the conductive particles are always very serious at this situation. Therefore, the final segregated CPCs usually have poor mechanical properties compared with the bulk polymer.[44]

Two different polymers have been used to solve the fusion properties of the segregated CPCs.[47–49] However, the improvement in mechanical properties is very limited because of the poor compatibility between two polymers. Recently, the addition of only 2.7 wt% high-density polyethylene (HDPE) was found to significantly increase their mechanical properties. For example, the strain, tear strength, and impact strength of the segregated carbon nanotube/ultrahigh-molecular-weight polyethylene (UHMWPE) composites showed a remarkable increase with values of 265, 61.9, and 167% compared with those of the conventional segregated materials, respectively, due to strong inter-diffusion and heat-sealing between the HDPE and UHMWPE molecules.[50] Meanwhile, chemically cross-linked polyolefin elastomer (POE) granules were used as the segregated phase and uncrosslinked POE/multi-walled carbon nanotubes (POE/MWCNTs) were used as the continuous phase to form segregated composites. The formed conductive elastomeric composites not only exhibited a low percolation threshold (from 9.0 to 1.5 vol%) but also enhanced mechanical properties (more than 12% and 30% increase in stress at 100% and 300% strain).[51] Inspired by these works, the problem of mechanical reduction for segregated CPCs probably can be solved by constructing segregated structures in two polymers with similar molecular structures but different viscosities. Besides, poly(L-lactide) (PLLA) has been attracting much interest in both industry and academia because of its attractive sustainability, biocompatibility, biodegradability, mechanical strength and easy processability.[52–55] In addition, the most important advantage of PLLA is that its viscosity can be tuned by controlling its molecular weight and crystallinity.[56–59] Therefore, it may be very easy to fabricate a segregated structure in the biodegradable PLLA with both high performance conductive and mechanical properties. However, fabrication of segregated structures using two PLLA polymers with different viscosities has not been reported.

In this work, two different PLLA polymers were used to fabricate biodegradable PLLA/MWCNT composites with segregated structures. One PLLA (H-PLLA) had a higher molecular weight, viscosity and crystallinity than the other (L-PLLA). The L-PLANT composites were obtained by melt-mixing L-PLLA with MWCNTs and then coated on the H-PLLA particles to construct the PLLA/MWCNT composites with segregated structures. The final PLLA/MWCNT composites exhibited ultralow percolation threshold, high-performance EMI shielding and enhanced mechanical properties, due to the continuous and dense MWCNT networks induced by segregated structures and higher interfacial interaction between H-PLLA and L-PLANT phases.

Experimental section

Materials

Two kinds of poly(L-lactide) (PLLA) with different viscosities were used in this work. One is of high viscosity with a melt flow index of 7.75 g/10 min at 190 °C and under 2.16 kg, denoted as H-PLLA. The H-PLLA (trade name 4032D) with 98.7 mol% L-isomeric content, a weight-average molecular weight (M_w) of 2.1×10^5 g mol^{-1} and a density of 1.24 g cm^{-3} was purchased from NatureWorks LLC (USA). The other is of low viscosity with a melt index of 30 g/10 min at 190 °C and under 2.16 kg, denoted as L-PLLA. The L-PLLA (trade name Hisun Revode 201) with 96.5 mol% L-isomeric content, a weight-average molecular weight (M_w) of 1.5×10^5 g mol^{-1} and a density of 1.25 g cm^{-3} was purchased from Zhejiang Hisun Biomaterials Co., Ltd, China. The MWCNTs (NC 7000) with an average diameter of 9.5 nm, an average length of 1.5 μm, a surface area of 250–300 m^2 g^{-1}, a density of 1.75 g cm^{-3} and a carbon purity of 90% were supplied by Nanocyl S.A. (Belgium).

Sample preparation

The H-PLLA and L-PLLA were dried at 60 °C for 48 h in a vacuum oven before use. The raw H-PLLA particles with a diameter of 30–50 mm were first pulverized using a high-speed mechanical pulverizer, and then meshed with a screening sifter. The pulverized granules with 40–60 meshes (250–425 μm) were annealed at 80 °C for 6 h to reach high crystallinity (35.8%, calculated on the basis of DSC results) for the segregated phase. The procedure for the segregated PLLA/MWCNT composites can be divided into three steps, Fig. 1. First, L-PLLA and MWCNTs with different loadings were melt-mixed in a rotational mixer (Hapro RM-200A) at 60 rpm for 5 min to obtain the L-PLANT master batches at 170 °C. Second, the 90 wt% H-PLLA granules and 10 wt% L-PLANT master batches were melt-mixed in the rotational mixer at 60 rpm for 5 min at 140 °C which is between the melting flow temperature of H-PLLA and L-PLLA. After mixing, the H-PLLA granules were coated with a thin layer of L-PLANT. In the last step, the coated H-PLLA granules were melt-compressed into sheets with a thickness of 1.5 mm

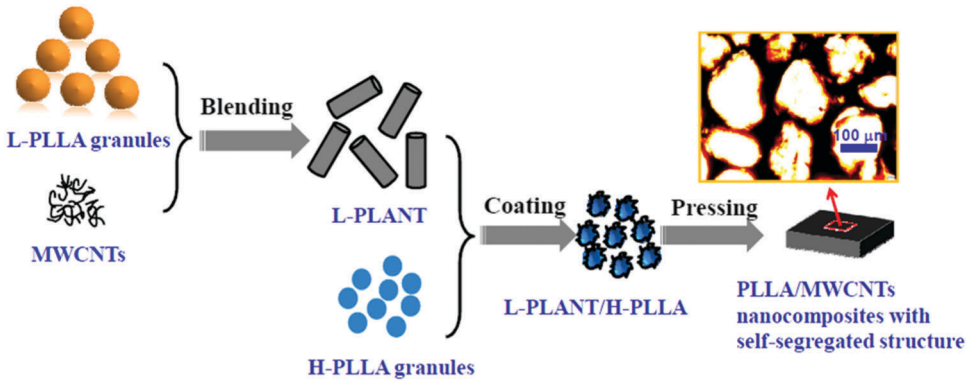

Fig. 1 Schematic description of the processing procedure for preparing the H-PLLA/L-PLANT composites with segregated structures.

at 10 MPa for 8 min to achieve the composites with segregated structures. The melt-compression temperature was set at 170 °C which was above the melting temperature of H-PLLA. For the comparison study, the 90 wt% H-PLLA granules and 10 wt% L-PLANT master batches were melt-mixed at 60 rpm for 5 min at 175 °C, and then melt-compressed into sheets with a thickness of 1.5 mm at 10 MPa at 170 °C to form the PLLA/MWCNT samples with a random distribution of MWCNTs. For convenience, the segregated PLLA/MWCNT composites and the samples with a random distribution of MWCNTs were marked as S-PLLA/MWCNTs and R-PLLA/MWCNTs, respectively.

Characterization

The nonisothermal crystallization behavior of H-PLLA and L-PLLA was performed using a differential scanning calorimeter (NETZSCH DSC-214) in a dry nitrogen atmosphere. For each measurement, about 5 mg of sample was placed in an aluminum pan, which was first heated from 25 to 190 °C at a heating rate of 10 °C min^{-1} and held for 5 min to remove the thermal history effect, then cooled down to 25 °C at a cooling rate of 10 °C min^{-1}, and finally reheated to 190 °C at a heating rate of 10 °C min^{-1}.

The rheological behavior of H-PLLA and L-PLLA was measured on a rotational rheometer (TA AR200ex) with two parallel plates. The dynamic frequency sweep mode was used with a strain of 1% from 0.0628 to 628 rad s^{-1} at 140 and 170 °C.

The electrical conductivity and percolation threshold of the samples were evaluated using a digital high resistance machine (PC68, Shanghai Precision Instrument Manufacture, China) at room temperature (23 °C). The electrical conductivity of the S-PLLA/MWCNT composites with 0.6 and 0.8 vol% MWCNTs and the R-PLLA/MWCNT composites with 0.8 vol% MWCNTs was conducted on a four-point probe instrument (RTS-8, Guangzhou Four-Point Probe Technology Co., Ltd, China) at room temperature. At least five specimens were tested and average data were reported.

The surface of the coated and uncoated H-PLLA granules, the segregated structures and MWCNT distribution in the samples were evaluated using a field-emission scanning electron microscope (SEM, JEOL, JSM-7800F). Before the SEM observation, the H-PLLA granules were directly coated with a layer of platinum in a vacuum chamber. While the composites were firstly cryo-fractured in liquid nitrogen, and then coated with a layer of platinum in a vacuum chamber. The segregated morphologies of the samples were also observed using an optical microscope (OM, Olympus BX51). Films with a thickness of 30 μm were cryo-microtomed from the PLLA/MWCNT composites with segregated structures.

Tensile tests were done using a Sansi CMT6503 Universal Testing Machine at a crosshead speed of 5 mm min^{-1} at 23 ± 2 °C. At least five specimens were tested for each sample, and the average results were evaluated.

The electromagnetic interference (EMI) shielding effectiveness (SE) of the composites was evaluated using an Agilent N5247A 10 MHz to 67 GHz PNA-x network analyzer at room temperature in the frequency range of 8.2–12.4 GHz. The samples with 12 mm diameter and 1.5 mm thickness were used for the test. The total EMI SE which summarizes the absorption shielding (SE_A), reflection shielding (SE_R), and multiple reflection shielding (SE_M) is also defined as the logarithmic ratio of incoming (P_{in}) to outgoing power (P_{out}) of electromagnetic radiation.[4,5,60]

$$SE_{total} = 10\log(P_{in}/P_{out}) = SE_A + SE_R + SE_M \quad (1)$$

Results and discussion

Phase morphology and MWCNT distribution in S-PLLA/MWCNT composites

Fig. 2 shows the melting behavior and rheological properties of two different PLLA polymers. Before annealing, the H-PLLA exhibits multiple transitions upon heating: a glass transition temperature (T_g) of ~60 °C, a cold crystallization peak (P_{cc}) of ~115 °C and a melting peak (P_m) of ~170 °C. However, the P_{cc} disappears and the T_g moves to a higher temperature of 65 °C after annealing. The crystallinity of H-PLLA, which is calculated using the obtained melting enthalpies to the melting enthalpies of 100% crystalline PLLA of 93.7 J g^{-1},[17] also increases from 2.8% before annealing to 35.9% after annealing. The results indicate that good crystallization in H-PLLA can be achieved by annealing. Fig. 2a also shows the melting behavior of L-PLLA without annealing. No P_{cc} and P_m were observed except only a T_g of 53 °C, suggesting the amorphous morphology of L-PLLA.

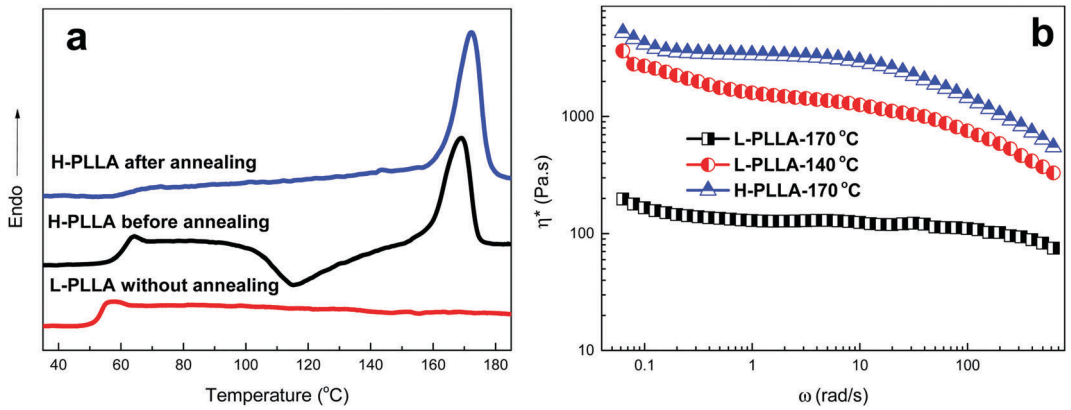

Fig. 2 (a) DSC first-melting curves and the (b) complex viscosity at 140 and 170 °C for the H-PLLA granules and L-PLLA samples.

Fig. 2b gives the complex viscosity of H-PLLA and L-PLLA at 140 °C (the coating temperature) and 170 °C (the melt-compression temperature). Because of the quasi-solid state of H-PLLA at 140 °C, we cannot give the rheological information of H-PLLA at this temperature. In fact, the complex viscosity of H-PLLA at 140 °C (quasi-solid state) can be supposed to be much higher than that of H-PLLA at 170 °C (melting state). However, L-PLLA can be melted into the melting state at 140 °C and show higher complex viscosity than that of L-PLLA at 170 °C, but still lower than that of H-PLLA at 170 °C, indicating that the complex viscosity of L-PLLA is much lower than that of H-PLLA at the same temperature. Furthermore, the quasi-solid state of H-PLLA and the melting state of L-PLLA at the coating temperature of 140 °C are thought to help the coating procedure.[47] The largely different viscosity at a melt-compression temperature of 170 °C will also retard the diffusion of MWCNTs into the H-PLLA phase.

Fig. 3 shows the uncoated and coated H-PLLA granules. It can be seen that the surface of the H-PLLA granule becomes smooth by coating with 10 wt% L-PLLA, indicating that H-PLLA granules can be well coated with a layer of L-PLLA at the mixing temperature of 140 °C. The L-PLANT with 0.5 vol% MWCNTs can also easily absorb on the H-PLLA surface and form a thin coating layer but with a rough surface (Fig. 3c), because of the MWCNT bundles at the coating layer (Fig. 3d). The successful coating is attributed to the largely different viscosity and the highly interfacial interaction between H-PLLA and L-PLLA. The good coating behavior will also lead to the well segregated structures in the nanocomposites.[48]

OM and SEM were performed to evaluate the formation of segregated structures and the conductive networks in the S-PLLA/MWCNT composites. As expected, the well segregated structures were achieved by choosing two PLLA polymers with different viscosities and temperature control. Fig. 4a and b shows the OM images of the S-PLLA/MWCNT composites with 0.05 and 0.6 vol% MWCNTs (*i.e.* 0.5 and 6 vol% in the L-PLLA phase), respectively. The black domains indicate the L-PLANT phase while the white domains represent the H-PLLA phase, because light cannot transmit through the L-PLANT domains.

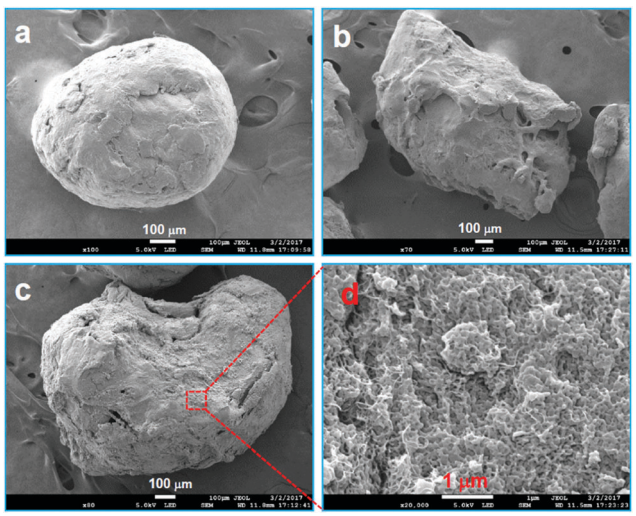

Fig. 3 SEM images of H-PLLA granules (a), L-PLLA coated PLLA granules (b), and L-PLANT with 0.5 vol% MWCNTs coated H-PLLA granules (c) and (d).

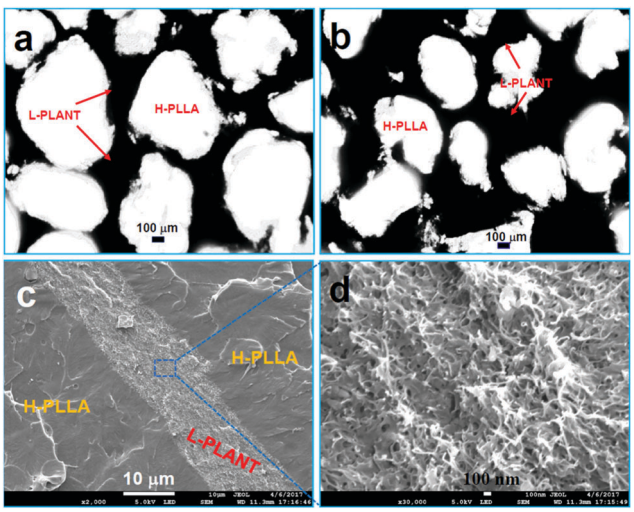

Fig. 4 OM images of the S-PLLA/MWCNT composites with MWCNT contents of (a) 0.05 vol% and (b) 0.6 vol%, and SEM micrographs of (c) S-PLLA/MWCNT composites with 0.6 vol% MWCNTs in the L-PLLA phase and (d) the magnification of (c).

It can be found that the H-PLLA phase is the segregated phase in the continuous L-PLANT phase, indicating that MWCNTs are selectively distributed in the L-PLANT phase and restricted to penetrate into the interior of the PLLA granules during processing. This unique structure also helps to form conductive networks as long as the L-PLANT phase is conductive. Furthermore, the well-defined segregated structures are found in both S-PLLA/MWCNT composites with 0.05 and 0.6 vol% MWCNTs, suggesting that the selective distribution of MWCNTs is regardless of MWCNT content. However, the denser MWCNTs are found in the S-PLLA/MWCNT composites with 0.6 vol% MWCNTs because of the darker L-PLANT domains. The SEM images give clearer images for the segregated structure and MWCNT dispersion. Fig. 4c shows the well-defined segregated structure of the S-PLLA/MWCNT composites with 0.6 vol% MWCNTs with an ~15 μm coating layer. Furthermore, no gaps were found at the interfaces between the L-PLANT phase and the H-PLLA phase, indicating the high interfacial interaction between the two phases. Fig. 4d also shows that the MWCNT bundles are well dispersed in the L-PLLA phase which will enhance the electrical conductivity of the composites.

Electrical conductivity of S-PLLA/MWCNT composites

Fig. 5 shows the electrical conductivity and percolation threshold behavior of the PLLA/MWCNT composites with segregated structures (S-PLLA/MWCNTs) and the random distribution of MWCNTs (R-PLLA/MWCNTs). The electrical conductivity of both S-PLLA/MWCNTs and R-PLLA/MWCNTs increases with increasing the content of MWCNT loadings. Furthermore, the increasing trends for both samples are the typical S-shaped curves. However, the electrical conductivity of the S-PLLA/MWCNT composites is higher than that of the R-PLLA/MWCNT composites at the same content of MWCNTs. For example, the electrical conductivity of S-PLLA/MWCNT composites with 0.1 vol% MWCNTs is 1.57×10^{-3} S m^{-1}, while the R-PLLA/MWCNT composites with 0.1 vol% MWCNTs can only reach 3.15×10^{-8} S m^{-1}. The electrical conductivity of S-PLLA/MWCNT composites can reach 25 S m^{-1}, while only 0.03 S m^{-1} for the R-PLLA/MWCNT composites with 0.8 vol% MWCNTs. The results indicate that the conductive properties of PLLA/MWCNT composites can be obviously improved by the fabrication of segregated structures therein. The high electrical conductivity of the S-PLLA/PCLNT nanocomposites is ascribed to the dense distribution of MWCNTs in the L-PLLA phase and the continuous L-PLANT networks formed by the segregated structures.

The classical percolation theory was also used to analyze the percolation threshold behavior of the S-PLLA/MWCNT and R-PLLA/MWCNT composites. The percolation threshold (ϕ_c) of the composites was achieved by fitting the variation of electrical conductivity (σ) with the volume content of MWCNTs (ϕ) as shown in eqn (2):[61]

$$\sigma = \sigma_0(\phi - \phi_c)^t \quad (2)$$

where σ_0 is a constant that is typically assigned to the plateau conductivity of fully loaded composites and t is the scaling exponent which is used to predict the mechanism of the conductive network. In theory, the values of $t \approx 1.3$ and $t \approx 2$ indicate two-dimensional and three-dimensional conductive networks, respectively. However, the experimental value of t ranges from 1 to 12.[19] The deviation between the theoretical prediction and the experimental value is still unclear. The most acceptable explanation is that the value of $t > 2$ means three-dimensional conductive networks while $t < 2$ indicates two-dimensional conductive networks formed in CPCs.[62–64] In this work, the value of t is 1.63 and 3.89 for the R-PLLA/MWCNT and S-PLLA/MWCNT composites, respectively (Fig. 5b), suggesting the presence of three-dimensional conductive networks in the S-PLLA/MWCNT composites but two-dimensional conductive networks in the R-PLLA/MWCNT composites. Therefore, the S-PLLA/MWCNT composites exhibit better electrical conductivity behavior than that of the R-PLLA/MWCNT composites.

As expected, the percolation threshold of PLLA/MWCNT composites is abruptly reduced by constructing the segregated structures. An ultralow percolation threshold of 0.019 vol% is found in the S-PLLA/MWCNT composites, while the percolation threshold of the R-PLLA/MWCNT composites is about

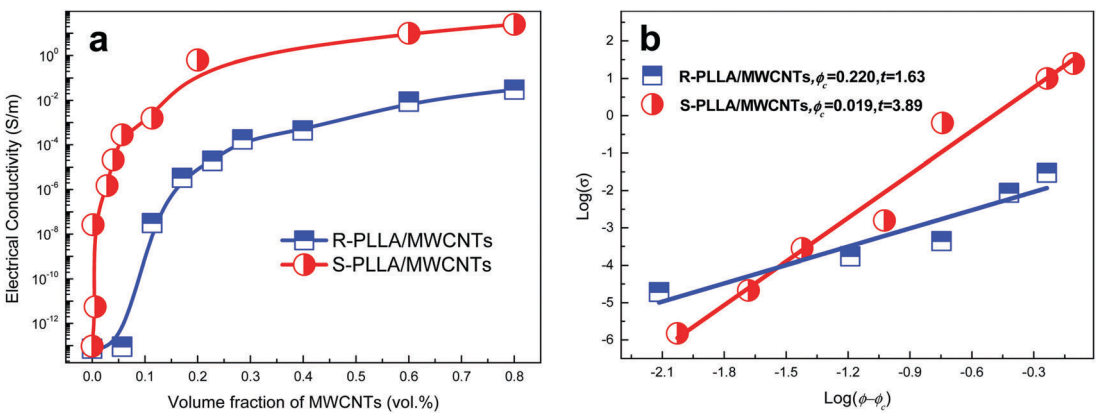

Fig. 5 (a) Electrical conductivity of the PLLA/MWCNT nanocomposites with a random distribution of MWCNTs and segregated structures as a function of MWCNT loadings, (b) the fitting lines of the nanocomposites using the classical percolation theory.

Table 1 Comparison of the electrical properties of the S-PLLA/MWCNT composites and reported PLLA/MWCNT composites

Processing method	Percolation threshold	MWCNT loading	Conductivity (S m^{-1})	Ref.
Melt mixing	0.35 wt%	2.0 wt%	10^{-5}	Quan *et al.*[65]
Melt mixing	0.5 wt%	1.0 wt%	10^{-3}	Kobashi *et al.*[66]
Electro-spinning	0.3 wt%	0.6 wt%	10^{-4}	McCullen *et al.*[67]
Solution mixing	13.5 wt%	20 wt%	0.1	Zhang *et al.*[68]
Melt mixing	0.48 vol%	—	—	Mai *et al.*[69]
Solution mixing	—	1.2 wt%	10^{-9}	Kim *et al.*[70]
Melt mixing	0.21 wt%	0.5 wt%	10^{-4}	Zhang *et al.*[17]
Melt mixing	3.0 wt%	5.0 wt%	0.1	Wang *et al.*[71]
Melt mixing	0.73 wt%	2.0 wt%	10	Huang *et al.*[72]
Solution mixing	0.495 wt%	5.0 wt%	1	Zhang *et al.*[73]
Melt mixing	0.1 wt%	5.0 wt%	1	Manfredi *et al.*[74]
Melt mixing	0.8 wt%	4.0 wt%	100	Li *et al.*[75]
Forming	0.16 vol%	5 wt%	0.16	Kuang *et al.*[76]
Melt mixing	0.5 wt%	2 wt%	~10	Villmow *et al.*[77]
Melt mixing	3 wt%	5 wt%	100	Wang *et al.*[78]
Segregated structure	0.04 vol%	1.0 wt%	12	Cui *et al.*[43]
Segregated structure	0.019 vol% (0.027 wt%)	0.8 vol% (1.1 wt%)	**25**	This work

0.22 vol% which is ~10.6 times higher than that of the S-PLLA/MWCNT composites. Table 1 shows the comparison of electrical properties for the S-PLLA/MWCNT composites and reported PLLA/MWCNT composites. It can be seen that our work has the lowest percolation threshold in comparison with the reported PLLA/MWCNT composites so far. The ultralow percolation threshold is ascribed to the continuous and dense MWCNT networks in the PLLA/MWCNT composites with segregated structures.

EMI shielding of S-PLLA/MWCNT composites

Fig. 6 shows the EMI SE_{total} of the S-PLLA/MWCNT and R-PLLA/MWCNT composites, as a function of MWCNT loading over the frequency of the X-band. It can be seen that the EMI SE_{total} of the PLLA/MWCNT composites increases with increasing the MWCNT loading. Furthermore, the enhancement in EMI SE_{total} becomes more obvious in the composites with segregated structures. A higher EMI SE_{total} value means more efficiency for attenuating microwave intensity. For example, the EMI SE_{total} of 20 dB implies the blocking of 99% incident microwave energy according to eqn (1), which is also required to be commercially applicable in EMI shielding devices.[79,80] For the R-PLLA/MWCNT composites, the EMI SE_{total} value >20 dB can be only found in the high MWCNT loading of 0.8 vol%. The average EMI SE_{total} values of the R-PLLA/MWCNT composites with 0.6 and 0.8 vol% MWCNTs is ~18 and ~22 dB, meaning that 98.42% and 99.37% microwave radiation can be blocked by the sample, respectively. However, for the S-PLLA/MWCNT composites with 0.6 and 0.8 vol% MWCNTs, the average EMI SE_{total} values of ~28 and ~30 dB can be achieved, corresponding to 99.84% and 99.90% blocking of microwave radiation, respectively. It can be found that the average EMI SE_{total} values of the S-PLLA/MWCNT composites are 1.56 and 1.36 times higher than those of the R-PLLA/MWCNT composites with 0.6 and 0.8 vol% MWCNTs, respectively.

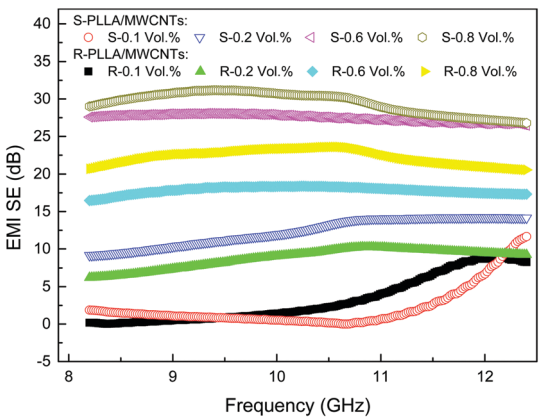

Fig. 6 The EMI SE_{total} as a function of frequency (X-band range) for S-PLLA/MWCNT and R-PLLA/MWCNT composites with different MWCNT loadings.

Table 2 also shows the comparison of the EMI SE_{total} for the S-PLLA/MWCNT composites and the reported polymer/MWCNT composites. It can be found that it is very difficult to obtain the polymer/MWCNT composites with high-performance EMI shielding (>20 dB) at low MWCNT loading (<2 wt%) and thin sample thickness (<2 mm). Here, the high EMI SE_{total} value (~30 dB) can be achieved in the S-PLLA/MWCNT composites with 1.1 wt% MWCNTs and 1.5 mm sample thickness. The high-performance EMI shielding of the S-PLLA/MWCNT composites is attributed to their high electrical conductivity and ultralow percolation threshold. It is well known that the free charges (electrons and holes) in conductive materials directionally move to produce the induced current during electromagnetic radiation.[6–11] The induced current can be quickly attenuated using resistance materials, leading to the blocking of electromagnetic radiation.[12–14] Thus, the high-performance EMI shielding can be achieved in the S-PLLA/MWCNT composites because of their high electrical conductivity.

The skin depth (δ) which is related to the electric field and the magnetic field of the materials is very important to evaluate the critical thickness for electrical conduction and EMI shielding. It has been reported that high-performance EMI shielding occurs at the thickness of the samples beyond the δ.[92] In other words, a higher δ value indicates worse EMI shielding of the materials. The δ value of the PLLA/MWCNT

Table 2 Comparison of EMI SE (in the X-Band) of the S-PLLA/MWCNT composites and reported polymer/MWCNT composites[a]

Polymer matrix	MWCNT loading	Thickness (mm)	EMI SE_{total} (dB)	Ref.
PLLA	0.8 vol% (1.1 wt%)	1.5	~**30**	This work
PLLA	1.0 wt%	0.9	~17.5	Cui *et al.*[43]
PLLA	3 wt%	2.5	~12	Kuang *et al.*[76]
PLLA	20 wt%	3.7	~19	Cui *et al.*[14]
PLLA/PCL	0.8 wt%	1.5	~18	Zhang *et al.*[35]
PA	2 wt%	1.5	~4	Li *et al.*[81]
PS	3.5 wt%	2.0	~10	Arjmand *et al.*[82]
PS	5 wt%	2.0	~17.2	Mahmoodi *et al.*[83]
PES	10 wt%	0.5	~26	Abbas *et al.*[84]
PTT	5 wt%	2.0	~23	Gupta *et al.*[85]
ABS	5 wt%	1.1	~25	Al-Saleh *et al.*[86]
PU	22 wt%	0.1	~25	Hoang *et al.*[87]
FCP	6 wt%	3.8	~22	Fletcher *et al.*[88]
PP	1.0 vol%	2.8	~4.6	Al-Saleh *et al.*[89]
PPCP	1.8 vol%	2.0	~23	Verma *et al.*[90]
PE	1.0 wt%	2.1	~17	Jia *et al.*[91]

[a] PCL: poly(ε-caprolactone); PA: polyacrylate; PS: polystyrene; PES: polyethersulfone; PTT: poly(trimethylene terephthalate); ABS: acrylonitrile-butadiene-styrene; PU: polyurethane; FCP: fluorocarbon polymer; PP: polypropylene; PPCP: polypropylene random copolymer; PE: polyethylene.

composites with various MWCNT loadings can be calculated using eqn (3).

$$\delta = \sqrt{\frac{1}{\pi f \mu \sigma}} \quad \text{when } \sigma \gg 2\pi f \varepsilon_0, \quad \mu = \mu_0 \mu_r \tag{3}$$

where ε_0, f, μ, μ_r, and μ_0 are the permittivity of free space (equal to 8.854×10^{-12} F m^{-1}), the frequency, the magnetic permeability of materials, the relative magnetic permeability of the conductive shield relative to that of free space ($\mu_r = 1$ in this case), and the permeability of free space (equal to $4\pi \times 10^{-7}$ H m^{-1}), respectively. The δ values at 8.2 GHz are 6.94, 1.75 and 1.11 mm for the S-PLLA/MWCNT composites with 0.2, 0.6 and 0.8 vol% MWCNTs, respectively. However, the δ value at 8.2 GHz is 32.09 mm for the R-PLLA/MWCNT composites with 0.8 vol% MWCNTs. The results indicate that the S-PLLA/MWCNT composites exhibit better EMI shielding than the R-PLLA/MWCNT composites. It is also found that only the δ value at 8.2 GHz of the S-PLLA/MWCNT composites with 0.8 vol% MWCNTs is lower than the thickness of our testing sample of 1.5 mm, indicating the highest efficiency for attenuating microwaves.

Furthermore, the EMI Shielding mechanism is mainly based on the reflection and absorption mechanisms. In a conductive material, the shielding by reflection (SE_R) can be expressed using eqn (4).[93]

$$SE_R = 168 + 10 \cdot \log \frac{\sigma_r}{\mu_r f} \tag{4}$$

where σ_r is the conductivity of the materials relative to the conductivity of copper, while the shielding by absorption (SE_A) which attenuates an electromagnetic wave through interaction with free charge carriers and/or electric/magnetic dipoles can be calculated using eqn (5).[38]

$$SE_A = 131 \cdot b \sqrt{f \mu_r \sigma_r} \tag{5}$$

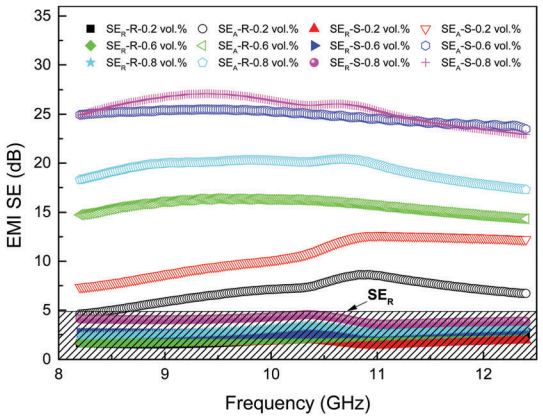

Fig. 7 Comparison of SE_A and SE_R as a function of frequency (X-band range) for S-PLLA/MWCNT and R-PLLA/MWCNT composites with different MWCNT loadings.

where b is the thickness of the sample. From eqn (4) and (5), it can be found that both SE_R and SE_A values increase with increasing σ_r, indicating that the higher conductivity can enhance both reflection and absorption. However, the SE_R decreases and SE_A increases with increasing μ_r, suggesting that the magnetic materials deteriorate the reflection loss and enhance the absorption. Here, the effect of μ_r can be omitted because of the weak magnetic response of the composites. In addition, the SE_A value is proportional to the thickness of the samples.

Fig. 7 shows the SE_A and SE_R values of the PLLA/MWCNT composites with different contents of MWCNTs in the X-band range. It can be found that the SE_A value significantly increases with increasing electrical conductivity, while the SE_R value shows a little enhancement in both S-PLLA/MWCNT and R-PLLA/MWCNT composites. The SE_R value of all the samples is very low (<5 dB) and the contribution of SE_R to SE_{total} is also very weak, indicating that the absorption is the major contribution to EMI shielding, particularly at high MWCNT loadings. For example, the SE_A and SE_R of the S-PLLA/MWCNT composites with 0.8 vol% are ~26 and ~4 dB, respectively. The shielding by absorption is over 5.5 times more than shielding by reflection. For R-PLLA/MWCNT composites with 0.8 vol%, the SE_A and SE_R values are ~19.5 and ~2.5 dB, showing that the contributions of absorption and reflection are 89% and 11%, respectively. The high percentage of absorption shielding is mainly ascribed to the high conductivity of MWCNTs where the free charges can move and attenuate during electromagnetic radiation.[38,93] It is worth noting that the SE_A value of the S-PLLA/MWCNT composites is higher than that of R-PLLA/MWCNT composites with the same MWCNT loading, which is mainly attributed to the abundant interfaces produced by the segregated structures. These interfaces can reflect and absorb the microwaves many times. Therefore, it is very difficult for the microwaves to escape from the sample before being absorbed.[43,76]

Mechanical properties of S-PLLA/MWCNT composites

Fig. 8 shows the mechanical properties of the S-PLLA/MWCNT and R-PLLA/MWCNT composites. It can be found that the

Young's modulus of the R-PLLA/MWCNT composites increases from 1017 to 1372 MPa with the MWCNT loadings increasing from 0 to 0.8 vol%. Furthermore, the Young's modulus of pure H-PLLA is 1078 MPa which is also lower than the PLLA/MWCNT composites with high contents of MWCNTs. The results indicate that the addition of MWCNTs can obviously enhance the modulus of the PLLA matrix. It is worth noting that the Young's modulus of the S-PLLA/MWCNT composites is much higher than that of the R-PLLA/MWCNT composites with the same MWCNT loading. For example, the Young's modulus of the S-PLLA/MWCNT composites is 15% higher than that of the R-PLLA/MWCNT composites with 0.6 vol% MWCNTs. The enhancements are attributed to the MWCNT network in the L-PLLA phase and the double continuous structure probably formed by the segregated strategy. The transcrystals which are formed by the nucleating effect of MWCNTs at the interfaces between the H-PLLA and L-PLANT phases (Fig. S1, ESI†) also contribute to the high Young's modulus.[94,95]

In addition, the tensile strength of the R-PLLA/MWCNT composites is also enhanced by the addition of MWCNTs. For example, the tensile strength of the R-PLLA/MWCNT composites increases from 53.2 to 62.7 MPa by the addition of 0.8 vol% MWCNTs. The results are ascribed to the high strength of MWCNTs and the nucleating effect of MWCNTs which increase the crystallinity of PLLA (Fig. S2, ESI†). The higher crystallinity usually results in a higher modulus and tensile strength.[17] However, the tensile strength of the S-PLLA/MWCNT composites increases at low MWCNT loadings (0, 0.06 and 0.2 vol%) and decreases at high MWCNT loadings (0.6 and 0.8 vol%). The decrease of tensile strength is ascribed to the high MWCNT concentration in the L-PLLA phase (~6.0 and ~8.0 vol%), which leads to serious stress concentration in the composites.[47]

Fig. 8c shows the elongation at break of the S-PLLA/MWCNT and R-PLLA/MWCNT composites. It can be seen that the elongation at break of R-PLLA/MWCNTs decreases upon increasing the MWCNT loading. However, the S-PLLA/MWCNT composites show higher elongation at break than the R-PLLA/MWCNT composites and pure PLLA. The results are ascribed to a double continuous structure induced by the segregated structure and the higher interfacial interaction between the H-PLLA and L-PLANT phases. Furthermore, the elongation at break of the S-PLLA/MWCNT composites increases abruptly at low MWCNT loading (0, 0.06 and 0.2 vol%) and then decreases at high content of MWCNTs (0.6 and 0.8 vol%) because of the serious stress concentration in the composites at high loadings.

The tensile fractured surface of the samples was also observed to evaluate their structural developments upon deformation. Fig. 9 shows a comparison study on the fractured surfaces of the R-PLLA/MWCNT and S-PLLA/MWCNT composites with 0.6 vol%. It can be found that the fractured surface of the e R-PLLA/MWCNT composites is much smoother than that of the S-PLLA/MWCNT composites with segregated structures.

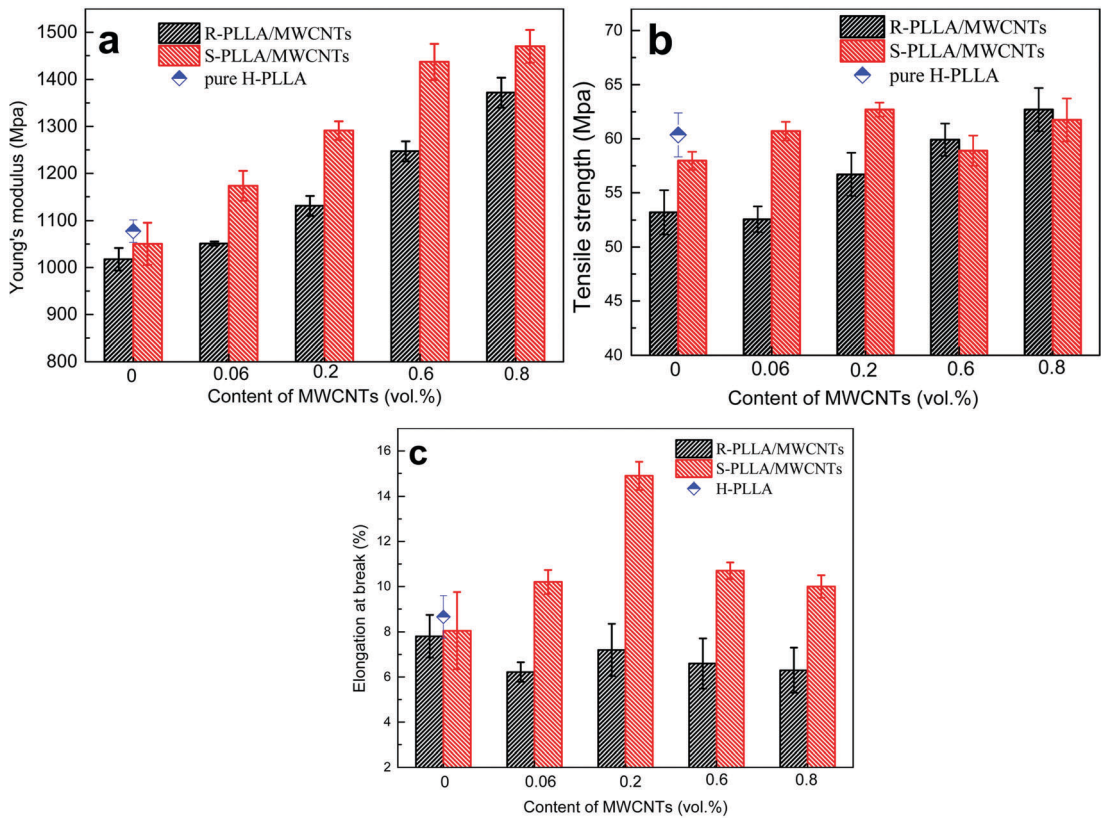

Fig. 8 Young's modulus (a), tensile strength (b) and elongation at break (c) of pure H-PLLA, the S-PLLA/MWCNT and R-PLLA/MWCNT composites with different contents of MWCNTs.

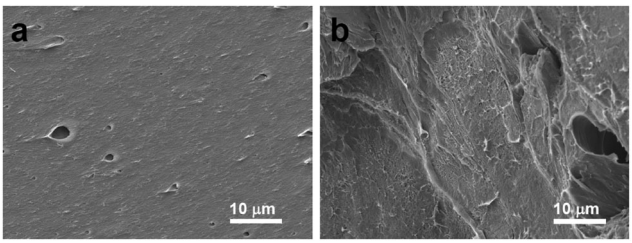

Fig. 9 SEM micrographs for the tensile fractured surface of the R-PLLA/MWCNT (a) and S-PLLA/MWCNT (b) composites with 0.6 vol% MWCNTs.

It is well-known that the rough fractured surface indicates the ductile fracture and the samples with good toughness.[47] The high toughness of the samples with segregated structures is also ascribed to the double continuous structures and the interfacial interaction between H-PLLA and L-PLANT.

Conclusion

In this work, PLLA/MWCNT nanocomposites with segregated structures were successfully fabricated by using two PLLA (L-PLLA and H-PLLA) polymers with different viscosities and crystallinities. The MWCNTs were confined to distribution in L-PLLA to form continuous MWCNT networks in the PLLA/MWCNT nanocomposites. The final nanocomposites with segregated structures (S-PLLA/MWCNTs) exhibited high electrical conductivity, ultralow percolation threshold and high performance EMI shielding effectiveness (SE) in comparison with PLLA/MWCNT composites with a random distribution of MWCNTs (R-PLLA/MWCNTs). For example, the electrical conductivity of the S-PLLA/MWCNT composites could reach 25 S m^{-1} with 0.8 vol% of MWCNT loading, while the R-PLLA/MWCNT composites had an electrical conductivity of only 0.03 S m^{-1} with the same content of MWCNTs. The percolation threshold of the S-PLLA/MWCNT composites was $\sim$0.019 vol%, which was only 8.6% of that of the R-PLLA/MWCNT composites with the percolation threshold of 0.22 vol%. The high-performance electrical properties mainly depended on the dense distribution of MWCNTs in the L-PLLA phase and the continuous L-PLANT networks formed by the segregated structures. The S-PLLA/MWCNT composites also exhibited higher EMI SE values than the R-PLLA/MWCNT composites at the same MWCNT loading. For example, the EMI SE value of the S-PLLA/MWCNT composites was $\sim$30 dB, which is 36% higher than that of the R-PLLA/MWCNT composites with 0.8 vol% MWCNT loading. The improvement in EMI SE is mainly attributed to the abundant interfaces produced by the segregated structures. These interfaces can reflect and absorb the microwaves many times. Furthermore, the Young's modulus, tensile strength and elongation at break of the S-PLLA/MWCNT composites were higher than those of the R-PLLA/MWCNT composites with the same content of MWCNTs, because of the continuous and dense MWCNT networks induced by the segregated structures and the higher interfacial interaction between the H-PLLA and L-PLANT phases. These approaches can be used to build other functional structural composites with other functional nanofillers or polymer matrices.[95,96]

Acknowledgements

The authors are grateful to the National Natural Science Foundation of China (51541306) and the Fundamental Research Funds for the Central Universities (XDJK2017B018, XDJK2017D051) for financial support of this work.

References

1 D. D. L. Chuang, *Carbon*, 2001, **39**, 279–285.
2 J.-J. Liang, Y. Wang, Y. Huang, Y.-F. Ma, Z.-F. Liu, J.-M. Cai, C.-D. Zhang, H.-J. Gao and Y.-S. Chen, *Carbon*, 2009, **47**, 922–925.
3 Y.-L. Yang and M. C. Gupta, *Nano Lett.*, 2005, **5**, 2131–2134.
4 M.-H. Al-Saleh and U. Sundararaj, *Carbon*, 2009, **47**, 1738–1746.
5 (*a*) Z.-F. Liu, G. Bai, Y. Huang, Y.-F. Ma, F. Du, F.-F. Li, T.-Y. Guo and Y.-S. Chen, *Carbon*, 2007, **45**, 821–827; (*b*) Z. Sun, L. Zhang, F. Dang, Y. Liu, Z. Fei, Q. Shao, H. Lin, J. Guo, L. Xiang, N. Yerra and Z. Guo, *CrystEngComm*, 2017, **19**, 3288–3298.
6 Z. Chen, C. Xu, C. Ma, W. Ren and H.-M. Cheng, *Adv. Mater.*, 2013, **25**, 1296–1300.
7 M. Arjmand, K. Chizari, B. Krause, P. Pötschke and U. Sundararaj, *Carbon*, 2016, **98**, 358–372.
8 J. Guo, H. Song, H. Liu, C. Luo, Y. Ren, T. Ding, M. A. Khan, D. P. Young, X. Liu, X. Zhang, J. Kong and Z. Guo, *J. Mater. Chem. C*, 2017, **5**, 5334–5344.
9 J. Li, H. Liu, J. Guo, Z. Hu, Z. Wang, B. Wang, L. Hiu, Y. Huang and Z. Guo, *J. Mater. Chem. C*, 2017, **5**, 1095–1105.
10 A. A. Eddib and D. D. L. Chung, *Carbon*, 2017, **117**, 427–436.
11 F. Shahzad, M. Alhabeb, C. B. Hatter, B. Anasori, S. M. Hong, C. M. Koo and Y. Gogotsi, *Science*, 2016, **353**, 1137–1140.
12 Y.-C. Qing, Q.-L. Wen, F. Luo, W.-C. Zhou and D.-M. Zhu, *J. Mater. Chem. C*, 2016, **4**, 371–375.
13 Z. Zeng, H. Jin, M. Chen, W. Li, L. Zhou and Z. Zhang, *Adv. Funct. Mater.*, 2016, **26**, 303–310.
14 C.-H. Cui, D.-X. Yan, H. Pang, L.-C. Jia, X. Xu, S. Yang, J.-Z. Xu and Z.-M. Li, *Chem. Eng. J.*, 2017, **323**, 29–36.
15 M. K. Vyas and A. Chandra, *ACS Appl. Mater. Interfaces*, 2016, **8**, 18450–18461.
16 S. Mondal, S. Ganguly, M. Rahaman, A. Aldalbahi, T. K. Chaki, D. Khastgir and N. C. Das, *Phys. Chem. Chem. Phys.*, 2016, **18**, 24591–24599.
17 K. Zhang, J.-K. Peng, Y.-D. Shi, Y.-F. Chen, J.-B. Zeng and M. Wang, *J. Phys. Chem. B*, 2016, **120**, 7423–7437.
18 W. Bauhofer and J. Z. Kovacs, *Compos. Sci. Technol.*, 2009, **69**, 1486–1498.
19 H. Deng, L. Lin, M. Ji, S. Zhang, M. Yang and Q. Fu, *Prog. Polym. Sci.*, 2014, **39**, 627–655.
20 J. Chen, Y.-Y. Shi, J.-H. Yang, N. Zhang, T. Huang, C. Chen, Y. Wang and Z.-W. Zhou, *J. Mater. Chem.*, 2012, **22**, 22398–22404.

21 Y. Lan, H. Liu, X.-H. Cao, S.-G. Zhao, K. Dai, X.-R. Yan, G.-Q. Zheng, C.-T. Liu, C.-Y. Shen and Z.-H. Guo, *Polymer*, 2016, **97**, 11–19.
22 A. Goeldel, A. Marmur, G. R. Kasaliwal, P. Poetschke and G. Heinrich, *Macromolecules*, 2011, **44**, 6094–6102.
23 E. Cohen, L. Zonder, A. Ophir, S. Kenig, S. McCarthy, C. Barry and J. Mead, *Macromolecules*, 2013, **46**, 1851–1859.
24 C. Hu, Z. Li, J. Gao, K. Dai, G. Zheng, C. Liu, C. Shen, H. Song and Z. Guo, *J. Mater. Chem. C*, 2017, **5**, 2318–2328.
25 H. Liu, J. Gao, W. Huang, K. Dai, G. Zheng, C. Liu, C. Shen, X. Yan, J. Guo and Z. Guo, *Nanoscale*, 2016, **8**, 12977–12989.
26 X. Guan, G. Zheng, K. Dai, C. Liu, X. Yan, C. Shen and Z. Guo, *ACS Appl. Mater. Interfaces*, 2016, **8**, 14150–14159.
27 H. Liu, W. Huang, J. Gao, K. Dai, G. Zheng, C. Liu, C. Shen, X. Yan, J. Guo and Z. Guo, *Appl. Phys. Lett.*, 2016, **108**, 011904.
28 Q.-H. Zhang and D.-J. Chen, *J. Mater. Sci.*, 2004, **39**, 1751–1757.
29 M. K. Seo and S. J. Park, *Chem. Phys. Lett.*, 2004, **395**, 44–48.
30 A. Ingo, L. Dirk, M. Sergej and P. P. Dudkin, *Polymer*, 2007, **48**, 1020–1029.
31 H. Xiu, Y. Zhou, C.-M. Huang, H.-W. Bai, Q. Zhang and Q. Fu, *Polymer*, 2016, **82**, 11–21.
32 G. Nasti, G. Gentile, P. Cerruti, C. Carfagna and V. Ambrogi, *Polymer*, 2016, **99**, 193–203.
33 I. Otero-Navas, M. Arjmand and U. Sundararaj, *Polymer*, 2017, **114**, 122–134.
34 J. Chen, X. Cui, K. Sui, Y. Zhu and W. Jiang, *Compos. Sci. Technol.*, 2017, **140**, 99–105.
35 K. Zhang, H. O. Yu, Y. D. Shi, Y. F. Chen, J. B. Zeng, J. Guo, B. Wang, Z. Guo and M. Wang, *J. Mater. Chem. C*, 2017, **5**, 2807–2817.
36 L. Q. Zhang, B. Yang, J. Teng, J. Lei, D. X. Yan, G. J. Zhong and Z. M. Li, *J. Mater. Chem. C*, 2017, **5**, 3130–3138.
37 M.-K. Li, C.-X. Gao, H.-L. Hu and Z.-D. Zhao, *Carbon*, 2013, **65**, 371–373.
38 F. Sharif, M. Arjmand, A. A. Moud, U. Sundararaj and E. P. L. Roberts, *ACS Appl. Mater. Interfaces*, 2017, **9**, 14171–14179.
39 H. Pang, L. Xu, D.-X. Yan and Z.-M. Li, *Prog. Polym. Sci.*, 2014, **39**, 1908–1933.
40 Y. Lin, S.-Q. Liu and L. Liu, *J. Mater. Chem. C*, 2016, **4**, 2353–2358.
41 H. Pang, Y. Bao, L. Xu, D.-X. Yan, W.-Q. Zhang, J.-H. Wang and Z.-M. Li, *J. Mater. Chem. A*, 2013, **1**, 4177–4181.
42 J.-H. Du, L. Zhao, Y. Zeng, L.-L. Zhang, F. Li, P.-F. Liu and C. Liu, *Carbon*, 2011, **49**, 1094–1100.
43 C.-H. Cui, D.-H. Yan, H. Pang, X. Xu, L.-C. Jia and Z.-M. Li, *ACS Sustainable Chem. Eng.*, 2016, **4**, 4137–4145.
44 S. Li, X. Li, C. Chen, H. Wang, Q. Deng, M. Gong and D. Li, *Compos. Sci. Technol.*, 2016, **132**, 31–37.
45 Y. Lan, H. Liu, X. Cao, S. Zhao, K. Dai, X. Yan, G. Zheng, C. Liu, C. Shen and Z. Guo, *Polymer*, 2016, **97**, 11–19.
46 M. Wang, K. Zhang, X. Dai, Y. Li, J. Guo, H. Liu, G. Li, Y. Tan, J. Zeng and Z. Guo, *Nanoscale*, 2017, **9**, 11017–11026.
47 (*a*) Y. D. Shi, M. Lei, Y. F. Chen, K. Zhang, J. B. Zeng and M. Wang, *J. Phys. Chem. C*, 2017, **121**, 3087–3098; (*b*) Y. Zheng, Y. Zheng, S. Yang, Z. Guo, T. Zhang, H. Song and Q. Shao, *Green Chem. Lett. Rev.*, 2017, **10**(4), 202–209.
48 S.-M. Zhang, H. Deng, Q. Zhang and Q. Fu, *ACS Appl. Mater. Interfaces*, 2014, **6**, 6835–6844.
49 X. J. Zha, T. Li, R. Y. Bao, L. Bai, Z. Y. Liu, W. Yang and M. B. Yang, *Compos. Sci. Technol.*, 2017, **139**, 17–25.
50 H. Pang, D.-X. Yan, Y. Bao, J.-B. Chen, C. Chen and Z.-M. Li, *J. Mater. Chem.*, 2012, **22**, 23568–23575.
51 T. Li, L.-F. Ma, R.-Y. Bao, G.-Q. Qi, W. Yang, B.-H. Xie and M.-B. Yang, *J. Mater. Chem. A*, 2015, **3**, 5482–5490.
52 (*a*) A. Södergård and M. Stolt, *Prog. Polym. Sci.*, 2002, **27**, 1123–1163; (*b*) C. Wang, Y. Wu, Y. Li, Q. Shao, X. Yan, C. Han, Z. Wang, Z. Liu and Z. Guo, *Polym. Adv. Technol.*, 2017, DOI: 10.1002/pat.4105; (*c*) W. Yang, X. Wang, J. Li, X. Yan, S. Ge, S. Tadakamalla and Z. Guo, *Polym. Eng. Sci.*, 2017, DOI: 10.1002/pen.24675; (*d*) Y. Li, X. Wu, J. Song, J. Li, Q. Shao, N. Cao, N. Lu and Z. Guo, *Polymer*, 2017, **124**, 41–47.
53 J. M. Raquez, Y. Habibi, M. Murariu and P. Dubois, *Prog. Polym. Sci.*, 2013, **38**, 1504–1542.
54 M. Wang, Y. Wu, Y. D. Li and J. B. Zeng, *Polym. Rev.*, 2017, DOI: 10.1080/15583724.2017.1287726.
55 J. B. Zeng, K. A. Li and A. K. Du, *RSC Adv.*, 2015, **5**, 32546–32565.
56 H. Y. Yin, X. F. Wei, R. Y. Bao, Q. X. Dong, Z. Y. Liu, W. Yang, B. H. Xie and M. B. Yang, *ACS Sustainable Chem. Eng.*, 2015, **3**, 654–661.
57 H. Y. Yin, X. F. Wei, R. Y. Bao, Q. X. Dong, Z. Y. Liu, W. Yang, B. H. Xie and M. B. Yang, *CrystEngComm*, 2015, **17**, 2310–2320.
58 J. R. Dorgan, H. Lehermeier and M. Mang, *J. Polym. Environ.*, 2000, **8**, 1–9.
59 J. J. Cooper-White and M. E. Mackay, *J. Polym. Sci., Part B: Polym. Phys.*, 1999, **37**, 1803–1814.
60 C. S. Zhang, Q. Q. Ni, S. Y. Fu and K. Kurashiki, *Compos. Sci. Technol.*, 2007, **67**, 2973–2980.
61 D. Stauffer and A. Aharony, *Introduction to percolation theory*, London, 1992.
62 J. P. Clerc, G. Giraud, J. M. Laugier and J. M. Luck, *Adv. Phys.*, 1990, **39**, 191–309.
63 V. M. Sonia, G. Claudio, M. Thomas, S. Sigfrid and R. Peter, *Phys. Rev. B: Condens. Matter Mater. Phys.*, 2005, **71**, 064201.
64 R. Zhang, M. Baxendale and T. Peijs, *Phys. Rev. B: Condens. Matter Mater. Phys.*, 2007, **76**, 195433.
65 H. Quan, S.-J. Zhang, J.-L. Qiao and L.-Y. Zhang, *Polymer*, 2012, **53**, 4547–4552.
66 K. Kobashi, T. Villmow, T. Andres and P. Pötschke, *Sens. Actuators, B*, 2008, **134**, 787–795.
67 S. D. McCullen, K. L. Stano, D. R. Stevens, W. A. Roberts, N. A. M. Riviere, L. I. Clarke and R. E. Gorga, *J. Appl. Polym. Sci.*, 2007, **105**, 1668–1678.
68 D.-H. Zhang, M. A. Kandadai, J. Cech, S. Roth and S. A. Curran, *J. Phys. Chem. B*, 2006, **110**, 12910–12915.
69 F. Mai, Y. Habibi, J. M. Raquez, P. Dubois, J. F. Feller, T. Peijs and E. Bilotti, *Polymer*, 2013, **54**, 6818–6823.
70 H. S. Kim, Y. S. Chae, B. H. Park, J. S. Yoon, M. Kang and H. J. Jin, *Curr. Appl. Phys.*, 2008, **8**, 803–806.

71 L.-J. Wang, J.-H. Qiu, E. Sakai and X. W. Wei, *Composites, Part A*, 2016, **89**, 18–25.
72 C. Huang, H. Bai, H. Xiu, Q. Zhang and Q. Fu, *Compos. Sci. Technol.*, 2014, **102**, 20–27.
73 D. Zhang, X. Liu and G. Wu, *Compos. Sci. Technol.*, 2016, **128**, 8–16.
74 E. Manfredi, F. Meyer, P. Verge, J.-M. Raquez, J.-M. Thomassin, M. Alexandre, B. Dervaux, F. DuPrez, P. V. D. Voort, C. Jerome and P. Dubois, *J. Mater. Chem.*, 2011, **21**, 16190–16196.
75 Q.-F. Li, Y. Xu, J.-S. Yoon and G.-X. Chen, *J. Mater. Sci.*, 2011, **46**, 2324–2330.
76 T. Kuang, L. Chang, F. Chen, Y. Sheng, D. Fu and X. Peng, *Carbon*, 2016, **105**, 305–313.
77 T. Villmow, P. Pötschke, S. Pegel, L. Häussler and B. Kretzschmar, *Polymer*, 2008, **49**, 3500–3509.
78 L. Wang, J. Qiu, E. Sakai and X. Wei, *Composites, Part A*, 2016, **89**, 18–25.
79 A. A. Moud, A. Javadi, H. Nazockdast, A. Fathi and V. Altstaedt, *J. Polym. Sci., Part B: Polym. Phys.*, 2015, **5**, 368–378.
80 M. Arjmand, A. A. Moud, Y. Li and U. Sundararaj, *RSC Adv.*, 2015, **5**, 56590–56598.
81 Y. Li, C. Chen, S. Zhang, Y. Ni and J. Huang, *Appl. Surf. Sci.*, 2008, **254**, 5766–5771.
82 M. Arjmand, T. Apperley, M. Okoniewski and U. Sundararaj, *Carbon*, 2012, **50**, 5126–5134.
83 M. Mahmoodi, M. Arjmand, U. Sundararaj and S. Park, *Carbon*, 2012, **50**, 1455–1464.
84 N. Abbas and H. T. Kim, *Macromol. Res.*, 2016, **24**, 1084–1090.
85 A. Gupta and V. Choudhary, *Compos. Sci. Technol.*, 2011, **71**, 1563–1568.
86 M. H. Al-Saleh and U. Sundararaj, *J. Polym. Sci., Part B: Polym. Phys.*, 2012, **50**, 1356–1362.
87 A. S. Hoang, *Adv. Nat. Sci.: Nanosci. Nanotechnol.*, 2011, **2**, 025007.
88 A. Fletcher, M. C. Gupta, K. L. Dudley and E. Vedeler, *Compos. Sci. Technol.*, 2010, **70**, 953–958.
89 L. C. Jia, D. X. Yan, C. H. Cui, X. Jiang, X. Ji and Z. M. Li, *J. Mater. Chem. C*, 2015, **3**, 9369–9378.
90 M. H. Al-Saleh and U. Sundararaj, *Carbon*, 2009, **47**, 1738–1746.
91 P. Verma, P. Saini, R. S. Malik and V. Choudhary, *Carbon*, 2015, **89**, 308–317.
92 W. L. Song, M. S. Cao, M. M. Lu, S. Bi, C. Y. Wang, J. Liu, J. Yuan and L. Z. Fan, *Carbon*, 2014, **66**, 67–76.
93 C. R. Paul, *Introduction to Electromagnetic Compatibility*, John Wiley & Sons Inc., NJ, 2nd edn, 2005.
94 F. Qiu, M. Wang, Y. Hao and S. Guo, *Composites, Part A*, 2014, **58**, 7–15.
95 M. Wang, L. Lin, Q. Peng, W. Ou and H. Li, *J. Appl. Polym. Sci.*, 2014, **131**, 39632.
96 (*a*) K. Zhang, G. Li, L. Feng, N. Wang, J. Guo, K. Sun, K. Yu, J. Zeng, T. Li, Z. Guo and M. Wang, *J. Mater. Chem. A*, 2017, DOI: 10.1039/C7TA05123A; (*b*) L. Zhang, W. Yu, C. Han, J. Guo, Q. Zhang, H. Xie, Q. Shao, Z. Sun and Z. Guo, *J. Electrochem. Soc.*, 2017, **164**, H651–H656; (*c*) K. Sun, P. Xie, Z. Wang, T. Su, Q. Shao, J. Ryu, X. Zhang, J. Guo, A. Shankar, J. Li, R. Fan, D. Cao and Z. Guo, *Polymer*, 2017, **125**, 50–57.